Inorganic Chemistry

Article

pubs.acs.org/IC

Absence of Colossal Magnetoresistance in the Oxypnictide $PrMnAsO_{0.95}F_{0.05}$

Eve J. Wildman,[†] Falak Sher,[‡] and Abbie C. Mclaughlin*,[†]

[†]The Chemistry Department, University of Aberdeen, Meston Walk, Aberdeen AB24 3UE, Scotland

[‡]Department of Chemistry, SBA School of Science and Engineering, LUMS, 54792 Lahore, Pakistan

ABSTRACT: We have recently reported a new mechanism of colossal magnetoresistance (CMR) in electron doped manganese oxypnictides $NdMnAsO_{1-x}F_x$. Magnetoresistances of up to −95% at 3 K have been observed. Here we show that upon replacing Nd for Pr, the CMR is surprisingly no longer present. Instead a sizable negative magnetoresistance is observed for $PrMnAsO_{0.95}F_{0.05}$ below 35 K (MR_{7T} (12 K) = −13.4% for $PrMnAsO_{0.95}F_{0.05}$). A detailed neutron and synchrotron X-ray diffraction study of $PrMnAsO_{0.95}F_{0.05}$ has been performed, which shows that a structural transition, T_s, occurs at 35 K from tetragonal *P4/nmm* to orthorhombic *Pmmn* symmetry. The structural transition is driven by the Pr 4f electrons degrees of freedom. The sizable −MR observed below the transition most likely arises due to a reduction in magnetic and/or multipolar scattering upon application of a magnetic field.

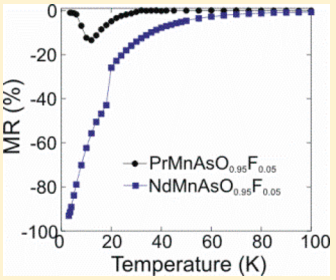

INTRODUCTION

Due to the recent discovery of high temperature superconductivity at 26 K in the electron doped 1111 iron pnictide LnFeAsO[1] there has been much active research into oxypnictide materials.[2] Superconducting transition temperatures (T_c) of ≤ 56.3 K have been achieved via the substitution of oxygen with fluorine,[3−5] by the creation of oxygen vacancies,[6] or by Th^{4+} substitution for Ln^{3+}.[7] These materials form with the primitive tetragonal ZrCuSiAs structure (space group *P4/nmm*), and various other transition metal analogues have been reported, for example LnMAsO (Ln = lanthanide, M = Mn, Co, Ni).[8−10] Recently, we reported colossal magnetoresistance (CMR) at low temperature in the antiferromagnetic oxypnictide series $NdMnAsO_{1-x}F_x$ (x = 0−0.08).[11] CMR is a rare phenomenon[12,13] which is well-known in other manganese oxides such as the perovskite $Ln_{1-x}A_xMnO_3$ (Ln = La, Pr and A = Sr, Ca)[14,15] and pyrochlore $Tl_2Mn_2O_7$.[16] Magnetoresistance (MR) is defined as the change of electrical resistivity ρ in an applied magnetic field **H**, so that MR = $(\rho(H) - \rho(0))/\rho(0)$. Magnetoresistant materials are important for magnetic memory device applications.

The parent compound NdMnAsO exhibits several magnetic transitions. At 359 K the Mn^{2+} spins align antiferromagnetically with moments aligned parallel to *c*. At 23 K (T_{Nd}) the Nd^{3+} spins order antiferromagnetically with their moments aligned parallel to the basal plane.[8,17] At the same time a spin reorientation of the Mn spins occurs; the Mn spins rotate from their previous alignment along the *c* axis to along *a* over a 3 K temperature interval. Doping with a small amount of fluorine to obtain phases of $NdMnAsO_{1-x}F_x$ drastically changes the electronic properties of the parent compound, but little change to the magnetic properties upon substitution were observed. Variable temperature powder neutron diffraction data showed antiferromagnetic order of the Mn^{2+} moments below 356(2) K, with the same magnetic structure as previously reported for NdMnAsO,[8,18] so there is no appreciable change in T_{Mn}. Below 23 K (T_{Nd}) antiferromagnetic alignment of Nd^{3+} spins along *a* was observed with a corresponding spin reorientation of Mn^{2+} into the basal plane at 20 K (T_{SR}), as described for NdMnAsO.[17] MR is observed below ∼75 K and is greatly enhanced upon cooling below T_{SR}, so that CMR is observed at low temperature (MR_{9T}(3K)) = −95%). Electron doping manganese pnictides with H^- has also been achieved with large negative magnetoresistance observed in the series $LaMnAsO_{1-x}H_x$. The maximum MR is observed in the sample x = 0.08 (MR_{5T}(8K) = −63%), as the antiferromagnetic order of Mn spins is suppressed by the emergence of a ferromagnetic metallic phase.[19] Electron doped materials $SmMnAsO_{1-x}$ have also been prepared,[20] and surprisingly a large positive magnetoresistance is observed at low temperature in metallic materials (MR ∼ 60% at 2 K for x = 0.3). This effect has been attributed to a field induced change of the complex Fermi surface. Given the diverse MR properties observed so far for the electron doped 1111 manganese oxyarsenides (Ln = La, Nd, Sm), we have synthesized and investigated the structural, electronic, and magnetic properties of $PrMnAsO_{0.95}F_{0.05}$.

EXPERIMENTAL SECTION

Polycrystalline samples of $PrMnAsO_{0.95}F_{0.05}$ and $NdMnAsO_{1-x}F_x$ (x = 0.02, 0.05) were synthesized via a two-step solid-state reaction method. Initially, the LnAs (Ln = Pr, Nd) precursor was obtained by the reaction of Ln pieces (Aldrich; 99.9%) and As (Alfa Aesar; 99.999%) at 900 °C for 24 h in an evacuated, sealed quartz tube. The resulting precursor was then reacted with stoichiometric amounts of MnO_2, Mn and MnF_2 (Aldrich; 99.99%); all powders were ground in an inert atmosphere and pressed into a pellet of 10 mm diameter. The pellet was placed into a Ta crucible and sintered at 1150 °C for 48 h, again in a quartz tube sealed under vacuum.

Received: October 6, 2014
Published: February 25, 2015

DOI: 10.1021/ic502445t
Inorg. Chem. 2015, 54, 2536−2542

Powder X-ray diffraction patterns of $PrMnAsO_{0.95}F_{0.05}$ and $NdMnAsO_{1-x}F_x$ (x = 0.02, 0.05) were collected using a Bruker D8 Advance diffractometer with twin Gobel mirrors and Cu Kα radiation. Data were collected at room temperature over the range 10° < 2θ < 100°, with a step size of 0.02°, and could be indexed on a tetragonal unit cell of space group $P4/nmm$, characteristic of the ZrCuSiAs structure type as previously reported for PrMnAsO.[21] X-ray diffraction patterns demonstrated that the material was of high purity.

High resolution synchrotron X-ray powder diffraction patterns were recorded on the ID31 beamline for $PrMnAsO_{0.95}F_{0.05}$ at ESRF, Grenoble, France at several temperatures between 10 and 290 K with a wavelength of 0.3999 Å and a collection time of 1 h at each temperature. The powder sample was inserted into a 0.5 mm diameter borosilicate glass capillary and spun at ∼1 Hz. The patterns were collected in the range 2° < 2θ < 50°.

Powder neutron diffraction data were also recorded for $PrMnAsO_{0.95}F_{0.05}$ using the D20 high intensity diffractometer at the Institute Laue Langevin (ILL, Grenoble, France). Neutrons of wavelength 2.4188 Å were incident on an 8 mm vanadium can, and data were recorded between 2 and 300 K in a cryostat and between 300 and 360 K in a furnace, with a collection time of 20 min at each temperature. The temperature dependency of the magnetic structure was obtained by Rietveld refinement[22] of the neutron data using the GSAS package.[23]

The temperature and field dependence of the electrical resistance were recorded using a Quantum Design physical property measurement system (PPMS) between 4 and 300 K in magnetic fields of 7 T. The magnetic susceptibility was measured with a Quantum Design superconducting quantum interference device magnetometer (SQUID). Zero field cooled (ZFC) measurements were recorded between 2 and 400 K in a field of 1000 Oe.

RESULTS

Crystal Structure. The Rietveld refinement of high resolution X-ray powder diffraction data collected between 10 and 290 K confirmed that $PrMnAsO_{0.95}F_{0.05}$ crystallizes at room temperature with the expected ZrCuSiAs-type tetragonal structure of space group $P4/nmm$ (Figure 1). Similar to

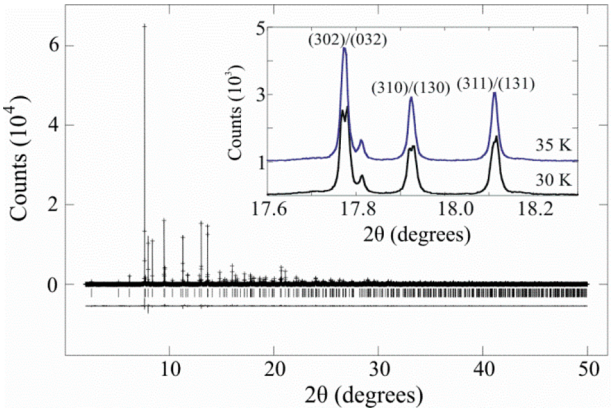

Figure 1. Rietveld refinement fit to the 10 K ID31 synchrotron X-ray powder diffraction pattern of $PrMnAsO_{0.95}F_{0.05}$. The inset shows the orthorhombic peak splitting as a function of temperature.

PrMnSbO,[24] a structural transition to orthorhombic $Pmmn$ symmetry is observed below T_s ∼ 35 K, demonstrated by a subtle splitting of the (302), (310), and (311) reflections upon cooling as shown in the inset of Figure 1. Pr^{3+} has the $4f^2$ configuration, and the structural distortion is a result of multipolar order, most likely ferromultipolar order as previously reported for PrMnSbO.[24] In contrast, there is no evidence of a structural transition in $NdMnAsO_{1-x}F_x$ which remains in the $P4/nmm$ space group down to 4 K.[11]

Below T_s ∼ 35 K the data were fit well with an orthorhombic unit cell of subgroup $Pmmn$ (a = 4.05896(1) Å, b = 4.06201(1) Å, and c = 8.89399(2) Å at 10 K) where the Pr site symmetry undergoes a reduction from $4mm$ to $mm2$. This structural change differs from the orthorhombic distortion observed in the Fe analogue, LaFeAsO, which results in an enlarged centered cell of space group $Cmma$. The refined values for lattice constants, atomic parameters, and selected bond lengths and angles with corresponding agreement indices for the respective variable temperature fits to the data are found in Table 1. There is no evidence of cation or As/O anion disorder. The Pr, Mn, and As occupancies refined to within ±1% of the full occupancy and were fixed at 1.0. The O and F occupancies were fixed at 0.95 and 0.05, respectively.

The temperature dependencies of the cell parameters are shown in Figure 2. The orthorhombic to tetragonal transition is clearly observed below T_s ∼ 35 K. The structural transition is driven by Pr 4f electron degrees of freedom[24] which results in the splitting of the Pr−O bond lengths. At 35 K the Pr−O bond length is 2.3429(1) Å and splits into two bond lengths of 2.385(5) and 2.303(4) Å below T_s (Figure 3). In comparison a much smaller change is evident in the Mn−As bond lengths. There is also a contraction in both of the Pr−O−Pr and As−Mn−As blocks below this temperature (Table 1).

The variation of c with temperature is shown in the inset of Figure 2, and a subtle change in slope is apparent at ∼140 K. There is also a discontinuity present in a at this temperature (Figure 2). The Mn−As and Pr−O/F bond lengths and angles are shown in Figure 3 and Table 1, respectively. Subtle anomalies are observed in all of the Mn−As bond lengths and As−Mn−As angles at ∼140 K. In contrast, there is no evidence of a discontinuity in any of the Pr−O bond lengths or Pr−O−Pr bond angles.

Magnetic Structure. Powder neutron diffraction measurements were recorded over the temperature range 2−360 K. Below T_{Mn} = 340 K the (100) magnetic reflection is observed alongside a magnetic contribution to the intensity of the (101) and (102) structural peaks as a result of antiferromagnetic ordering of the Mn spins (Figure 4). This is comparable to the Nd analogue ($NdMnAsO_{0.95}F_{0.05}$) with a T_{Mn} = 356 K.[11] Above 340 K, the (100) magnetic reflection is no longer observable but diffuse scattering characteristic of short range ordering is still present as shown in Figure 4. The magnetic reflections observed below 340 K could be indexed with the propagation vector (k = 0, 0, 0), so that the nuclear and magnetic unit cells are equivalent. Rietveld refinement of the data revealed that at T_{Mn} the Mn moments align antiferromagnetically in the ab plane and ferromagnetically along c, as previously reported for $NdMnAsO_{1-x}F_x$,[8,11,17] with spins parallel to the c axis.

The variation of the high spin Mn moment with temperature is displayed in Figure 5. Below ∼220 K (T_{SR1}) the Mn spins start to reorient to align parallel to a, which results in a slight reduction in intensity of the (100) and (101) peaks but an increase in the intensity of the (102) reflection. There is no change in spin state of the Mn ion at the spin reorientation transition. At 180 K a poorer Rietveld fit to the (100) magnetic reflection is observed which can be modeled by adding a small antiferromagnetic moment on the Pr^{3+} site. The Pr^{3+} spins are aligned parallel to a (Figure 4), and the concave variation of the Pr moment with temperature (Figure 5) suggests that the magnetic ordering of the Pr^{3+} spins is induced upon

DOI: 10.1021/ic502445t
Inorg. Chem. 2015, 54, 2536−2542

Table 1. Refined Cell Parameters, Agreement Factors, Atomic Parameters, and Selected Bond Lengths and Angles for $PrMnAsO_{0.95}F_{0.5}$ from Rietveld Fits against ID31 Synchrotron Powder X-ray Diffraction Data at Various Temperatures[a]

Atom	Occupancy		Temperature (K) 10	15	20	25	30	35	40
Pr	1.00	z	0.13150(3)	0.13146(3)	0.13148(3)	0.13147(3)	0.13143(3)	0.13143(3)	0.13143(3)
		U_{iso} (Å^2)	0.00112(4)	0.00112(4)	0.00102(4)	0.00116(4)	0.00124(4)	0.00121(4)	0.00122(4)
Mn	1.00	z	0.5014(3)	0.5013(3)	0.5006(3)	0.5009(3)	0.5010(4)	0.5	0.5
		U_{iso} (Å^2)	0.0018 (1)	0.0020(1)	0.0020(1)	0.00197(12)	0.0022(1)	0.0019(1)	0.0020(1)
As	1.00	z	0.67299(5)	0.67297(5)	0.67300(5)	0.67298(5)	0.67289(5)	0.67288(5)	0.67292(6)
		U_{iso} (Å^2)	0.00149 (9)	0.00155(8)	0.00150(8)	0.00160(8)	0.00166(8)	0.00159(8)	0.00165(9)
O/F	0.95/0.05	z	0.008(1)	0.0084(9)	0.0097(9)	0.0092(9)	0.009(1)	0	0
		U_{iso} (Å^2)	0.0001(7)	0.0001(6)	0.0005(6)	0.0007(6)	0.0009(7)	0.0028(5)	0.0026(5)
		a (Å)	4.05896 (1)	4.059057(9)	4.059149(9)	4.059300(9)	4.05953(1)	4.060639(6)	4.060731(6)
		b (Å)	4.06201 (1)	4.061925(9)	4.061887(9)	4.061805(9)	4.06161(1)	-	-
		c (Å)	8.89399 (2)	8.89444(1)	8.89482(1)	8.89513(1)	8.89546(1)	8.89557(2)	8.89590(2)
		χ^2 (%)	2.785	3.926	3.597	3.355	3.133	3.108	2.967
		R_{WP} (%)	12.14	11.46	11.65	11.72	11.80	12.24	12.47
		R_P (%)	8.43	8.03	8.19	8.42	8.23	8.63	8.79
		Pr-O/F (Å)	2.378(5)	2.381(5)	2.388(4)	2.386(5)	2.385(5)	2.3429(1)	2.3429(1)
			2.309(5)	2.306(4)	2.301(4)	2.303(4)	2.303(4)	-	-
		Mn-As (Å)	2.556(1)	2.555(1)	2.551(1)	2.553(1)	2.553(2)	2.5470(3)	2.5473(3)
			2.539(1)	2.540(1)	2.544(1)	2.542(1)	2.542(2)	-	-
		Mn-Mn (Å)	2.87131(5)	2.87129(4)	2.87124(2)	2.87129(3)	2.87131(4)	2.87131(4)	2.87137(2)
		Pr-As (Å)	3.3567(3)	3.3570(3)	3.3568(3)	3.3570(3)	3.3577(3)	3.3578(3)	3.3577(3)
		α_1 Pr-O/F-Pr (°)	123.0(4)	123.3(4)	123.8(4)	123.6(4)	123.6(4)	120.13(1)	120.13(1)
			117.3(4)	117.0(4)	116.5(3)	116.7(4)	116.8(4)	-	-
		α_2 Pr-O/F-Pr (°)	104.37(1)	104.36(1)	104.34(1)	104.35(1)	104.34(1)	104.419(5)	104.420(5)
		α_1 As-Mn-As (°)	111.39(1)	111.391(9)	111.399(9)	111.396(9)	111.381(9)	111.38(1)	111.39(1)
		α_2 As-Mn-As (°)	106.1(1)	106.1(1)	105.8(1)	105.9(1)	106.0(1)	105.72(1)	105.70(1)
			105.3(1)	105.3(1)	105.5(1)	105.4(1)	105.4(1)	-	-
		MnAs Layer (Å)	3.0522(2)	3.0538(1)	3.0669(1)	3.0613(1)	3.0581(1)	3.0757(2)	3.0766(2)
		Pr(O/F) Layer (Å)	2.2039(2)	2.1891(1)	2.1664(1)	2.1752(1)	2.1781(1)	2.338(2)	2.3384(2)

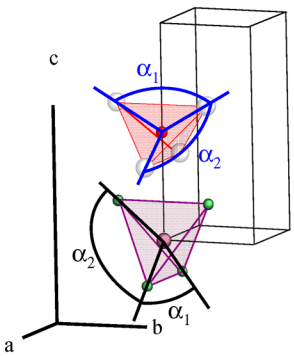

Atom	Occupancy		Temperature (K) 70	100	130	160	200	250	290
Pr	0.995	z	0.13143(3)	0.13135(3)	0.13139(3)	0.13135(3)	0.13124(3)	0.13123(3)	0.13119(3)
		U_{iso} (Å^2)	0.00174(5)	0.00199(4)	0.00295(5)	0.00291(4)	0.00359(5)	0.00445(5)	0.00501(5)
Mn	1.00	z	0.5	0.5	0.5	0.5	0.5	0.5	0.5
		U_{iso} (Å^2)	0.0027(1)	0.0030(1)	0.0042(1)	0.0043(1)	0.0052(1)	0.0066(1)	0.0075(1)
As	1.00	z	0.67291(6)	0.67291(5)	0.67280(6)	0.67277(6)	0.67287(6)	0.67301(6)	0.67295(6)
		U_{iso} (Å^2)	0.00227(9)	0.00264(8)	0.0038(1)	0.00398(9)	0.0048(1)	0.0060(1)	0.0067(1)
O/F	0.95/0.05	z	0	0	0	0	0	0	0
		U_{iso} (Å^2)	0.0034(6)	0.0034(5)	0.0059(7)	0.0042(6)	0.0039(6)	0.0045(6)	0.0051(6)
		a (Å)	4.061816(6)	4.062342(6)	4.062877(6)	4.063972(6)	4.065303(6)	4.067319(6)	4.068873(6)
		c (Å)	8.89837(2)	8.90023(1)	8.90198(2)	8.90543(1)	8.90982(2)	8.91620(1)	8.92088(1)
		χ^2 (%)	4.428	3.456	3.677	2.969	2.792	3.876	6.166
		R_{WP} (%)	12.73	11.04	12.53	11.55	11.86	11.24	10.94
		R_P (%)	9.59	8.13	9.01	8.19	8.39	8.14	7.65
		Pr-O/F (Å)	2.3436(1)	2.3436(1)	2.3441(1)	2.3446(1)	2.3450(1)	2.3463(1)	2.3470(1)
		Mn-As (Å)	2.5479(3)	2.5483(3)	2.5482(4)	2.5488(3)	2.5503(3)	2.5525(3)	2.5533(3)
		Mn-Mn (Å)	2.87214(2)	2.87251(3)	2.87289(1)	2.87366(1)	2.87460(2)	2.87603(1)	2.87713(4)
		Pr-As (Å)	3.3586(3)	3.3595(3)	3.3603(4)	3.3617(3)	3.3630(4)	3.3642(3)	3.3660(3)
		α_1 Pr-O-Pr (°)	120.13(1)	120.15(1)	120.14(1)	120.15(1)	120.18(1)	120.17(1)	120.18(1)
		α_2 Pr-O-Pr (°)	104.420(6)	104.409(5)	104.416(6)	104.412(6)	104.397(6)	104.401(6)	104.398(6)
		α_1 As-Mn-As (°)	111.39(1)	111.388(9)	111.37(1)	111.37(1)	111.39(1)	111.42(1)	111.42(1)
		α_2 As-Mn-As (°)	105.70(2)	105.70(1)	105.73(2)	105.73(2)	105.69(2)	105.64(2)	105.65(2)
		MnAs Layer (Å)	3.0772(2)	3.0779(1)	3.0765(2)	3.0772(1)	3.0805(2)	3.0852(1)	3.0857(1)
		Pr(O/F) Layer (Å)	2.3390(2)	2.3381(1)	2.3393(2)	2.3395(1)	2.3387(2)	2.3401(1)	2.3407(1)

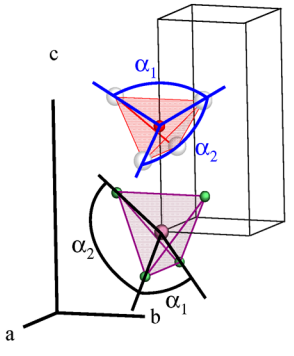

[a]Pr and As are at 2c (1/4, 1/4, *z*), Mn at 2b (3/4, 1/4, *z*), and O, F at 2a (3/4, 1/4, *z*). A structural transition from tetragonal *P*4/*nmm* to orthorhombic *Pmmn* symmetry is apparent below 35 K.

DOI: 10.1021/ic502445t
Inorg. Chem. 2015, 54, 2536−2542

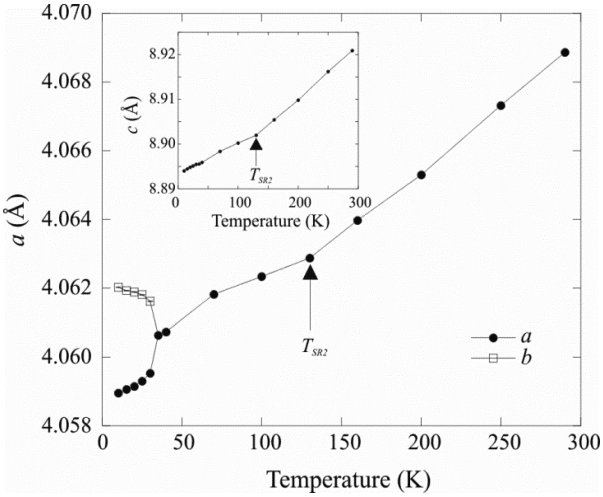

Figure 2. Temperature variation of the a and b cell parameters of $PrMnAsO_{0.95}F_{0.05}$with temperature, evidencing the structural transition below 35 K. The inset shows the variation of the c cell parameter with temperature. The temperature at which the Mn spins are fully aligned in the basal plane, T_{SR2}, is indicated on both panels by an arrow.

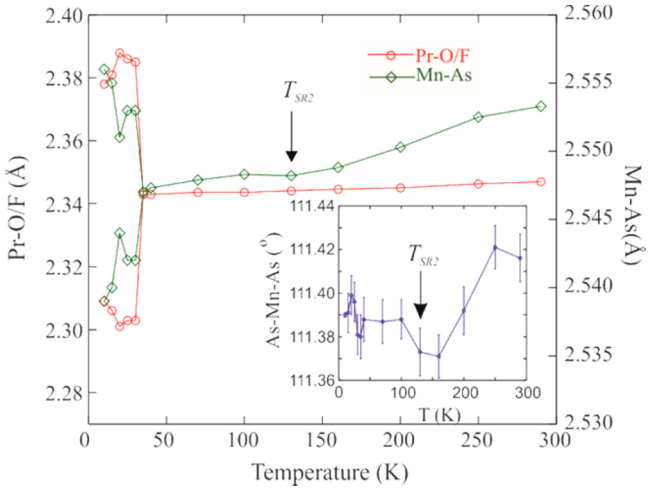

Figure 3. Variation of the Pr−O/F and Mn−As bond lengths with temperature. The inset shows the temperature variation of the As−Mn−As bond angle (α_1). The structural anomaly at T_{SR2} is indicated by an arrow.

reorientation of the Mn spins into the basal plane. The spin reorientation of the Mn moments occurs over an ∼80 K temperature interval so that by 140 K (T_{SR2}) the Mn spins are fully aligned parallel to a, with a moment of 3.17(3) μ_B. The same spin reorientation is observed below 90 K in PrMnSbO over a 20 K temperature interval.[24] For PrMnSbO, the induced Pr antiferromagnetic order is only observed once the Mn moments are fully aligned in the basal plane. In contrast, in $PrMnAsO_{0.95}F_{0.05}$, the induced Pr moment is detected after the Mn spins start reorienting into the basal plane. It is most likely that a small Pr moment is actually also induced at 200 K but the magnetic intensity is too weak to be seen in our measurements. Similar behavior is also observed in $La_{1-x}Ce_xMnAsO$[25] where spin reorientation of the Mn moments induces long range magnetic order of the Ce^{3+} moments below 34 K. A

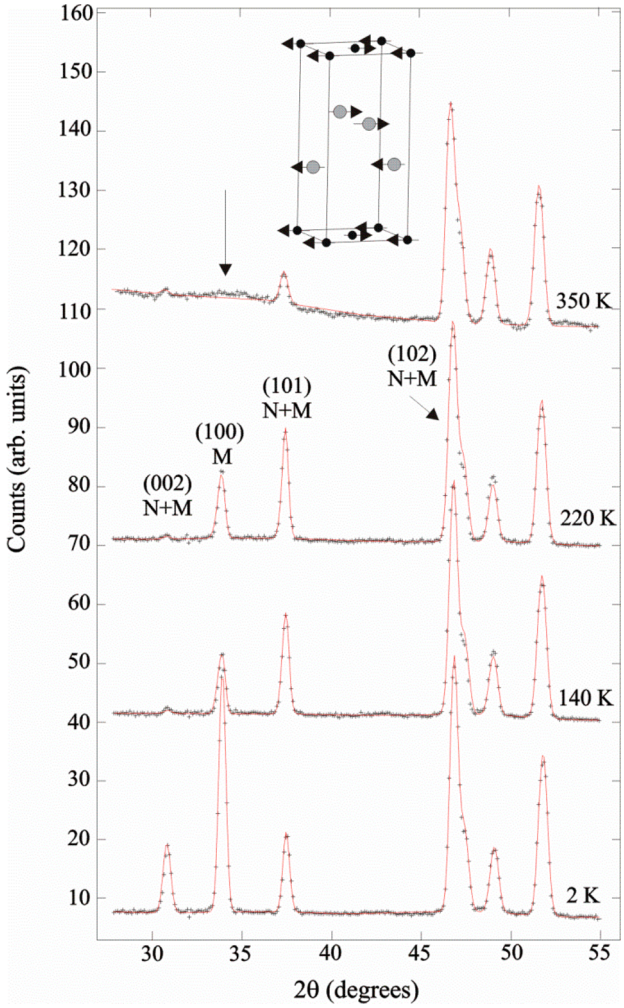

Figure 4. Portion of the D20 neutron diffraction pattern for $PrMnAsO_{0.95}F_{0.05}$ showing the magnetic diffraction peaks at several temperatures. The Rietveld fit to the data is shown. Diffuse scattering characteristic of short range magnetic order is still evident above T_{Mn} as indicated by the arrow. The inset shows the magnetic structure below T_{Pr}. The small black spheres are Mn, and the larger gray spheres are Pr.

simultaneous spin reorientation of the Mn moments and alignment of the Nd spins is also observed in $NdMnAsO_{1-x}F_x$ at the lower temperature of 23 K.[8,11,17]

Magnetic susceptibility measurements of $PrMnAsO_{0.95}F_{0.05}$ show an anomaly in the inverse susceptibility at $T_{Mn} \sim 340$ K and a broad transition around 38 K (Figure 6). There is no evidence of a magnetic transition in the neutron diffraction data at this temperature, so that the broad peak most likely arises from the crystalline field splitting of the Pr^{3+} ion.

The high resolution synchrotron X-ray diffraction data identified a structural transition at $T_s \sim 35$ K from tetragonal to orthorhombic symmetry, due to a small distortion in the ab plane (Figures 1 and 2). Since $a \neq b$ below this temperature, the neutron data were separately modeled with the moments along the a and b axes and then compared. The best results were obtained with magnetic moments ordered parallel to b (χ^2 = 13.3 for moments aligned along b compared to 14.1 for moments aligned along a at 2 K); this arrangement was

DOI: 10.1021/ic502445t
Inorg. Chem. 2015, 54, 2536−2542

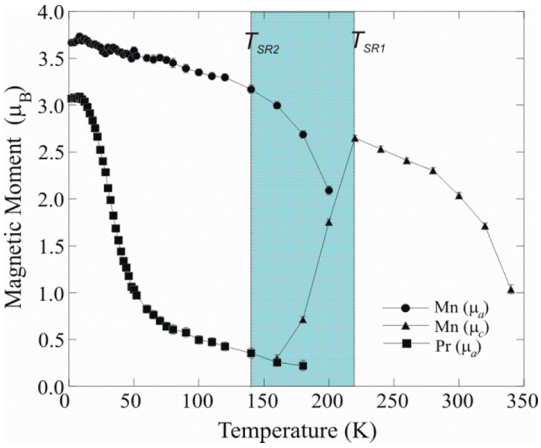

Figure 5. Temperature variation of the refined Mn and Pr moments for $PrMnAsO_{0.95}F_{0.05}$. The shaded region shows the spin reorientation of the Mn spins from parallel to c into the basal plane between T_{SR1} and T_{SR2}.

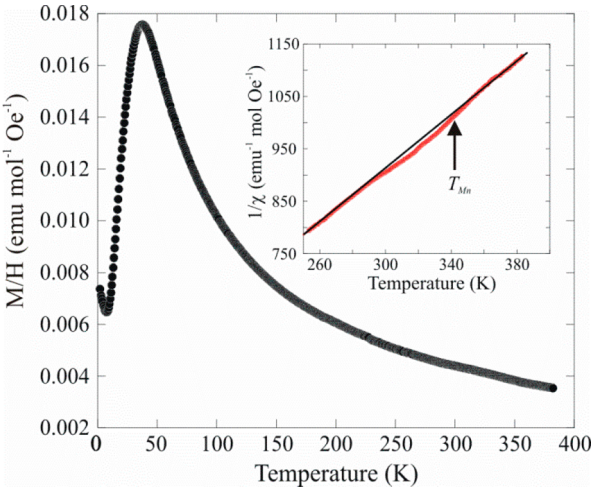

Figure 6. Direct current magnetic susceptibility of $PrMnAsO_{0.95}F_{0.05}$ measured as a function of temperature in a 1000 Oe magnetic field. The inset shows a section of the variation of the inverse susceptibility with temperature which evidences antiferromagnetic order of the Mn spins below 340 K. The bold black line is a linear fit to the inverse susceptibility data, and there is a clear deviation at T_{Mn}.

therefore adopted for all temperatures below T_s. The synchrotron data also evidenced anomalies in the cell parameters, Mn−As bond lengths and angles at ∼140 K (Figures 2 and 3, Table 1), which correspond to T_{SR2}, the temperature at which the Mn moments have fully reorientated into the basal plane. This demonstrates a coupling between the crystal and magnetic lattices; i.e., the crystal lattice is sensitive to the orientation of the Mn moment. In corroboration there is no evidence of a discontinuity in any of the Pr−O/F bond lengths or Pr−O−Pr bond angles at 140 K.

Electronic Properties. $PrMnAsO_{0.95}F_{0.05}$ is semiconducting with a room temperature resistivity of $\rho_{290\,K}$ = 0.304 Ω·cm. Arrhenius behavior is observed between 95 and 220 K (Figure 7, inset b), where the resistivity, ρ, follows the relationship $\rho = \rho_0 \exp(E_g/2kT)$ (where ρ is the measured resistivity, E_g the band gap, k the Boltzmann constant, and T the temperature), with a calculated E_g of 0.048(1) eV. The electron transport properties in this region are dominated by thermally activated charge

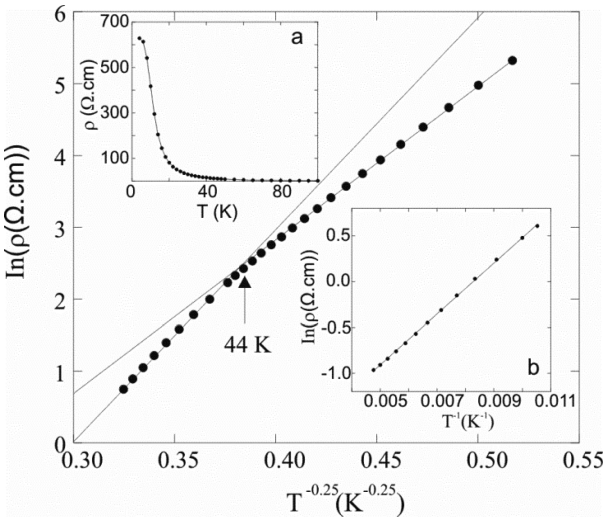

Figure 7. Plot of ln(resistivity) against $T^{-1/4}$ for $PrMnAsO_{0.95}F_{0.05}$ evidencing a subtle electronic transition at 44 K. The resistivity can be fit to the Mott VRH equation $\rho = \rho_0 \exp(T_0/T)^{1/4}$ over the whole temperature range shown. The insets show the variation of resistivity for $PrMnAsO_{0.95}F_{0.05}$ (inset a) and variation of ln(ρ) with inverse temperature showing that $PrMnAsO_{0.95}F_{0.05}$ exhibits Arrhenius behavior between 95 and 220 K (inset b).

carriers across a band gap. Similar results are obtained for $NdMnAsO_{0.95}F_{0.05}$,[11] where E_g = 0.023(1) eV.

The low temperature resistivity of $PrMnAsO_{0.95}F_{0.05}$ is shown in Figure 7, inset a. Upon cooling $PrMnAsO_{0.95}F_{0.05}$ below 95 K, the temperature variation of the resistivity data is characteristic of Mott three-dimensional variable range hopping (VRH) of the electrons (Figure 7).[26] Variable range hopping conductivity implies that the electronic states are localized at the Fermi level by disorder. Disorder in a solid can introduce random potential energy in the lattice which can lead to localization of the electronic wave function (Anderson localization). Anderson localization is caused by a disordered potential which could arise from the substitution of F^- for O^{2-} in $PrMnAsO_{0.95}F_{0.05}$. At low temperatures Anderson localization occurs in many metals and semiconductors where variable range hopping of the charge carriers is observed. In the variable range hopping mechanism, a localized electron can then only move from one localized site to another by phonon assisted hopping, which is a combined thermally active quantum tunneling process. An electron will only tunnel to another site if the thermal activation energy required for the hop is reduced. In this case the resistivity, ρ, can be modeled as $\rho = \rho_0 \exp(T_0/T)^{1/4}$. T_0 represents the localization temperature. T_0 depends on the radius of localized states α (also called the localization length), and the density of states at the Fermi level, $N(E_F)$ so that $T_0 = \lambda/[k_B N(E_F)\alpha^3]$; λ is a dimensionless constant.[27,28] Three-dimensional variable range hopping of the electrons is also observed for $NdMnAsO_{0.95}F_{0.05}$ below 75 K.[11] The resistivity data for $PrMnAsO_{0.95}F_{0.05}$ in Figure 7 is fit to the Mott three-dimensional VRH equation. A subtle electronic transition is evidenced at 44 K (Figure 7) as a change of slope is observed in the ln(ρ) versus $T^{-0.25}$ plot. This transition is not coincident with the structural transition at 35 K. The change of slope observed in the ln(ρ) versus $T^{-0.25}$ plot (Figure 7) suggests a crossover between two three-dimensional VRH states with different values of the localization temperature T_0 (T_0 = 6.16(1) × 10^5 and 2.08(1) × 10^5 K for the high and low

DOI: 10.1021/ic502445t
Inorg. Chem. 2015, 54, 2536−2542

temperature electronic states, respectively). This reveals that the material adopts a more disordered electronic state at higher temperatures as T_0, which represents the degree of electronic disorder, is larger. T_0 is large for the $LnMnAsO_{1-x}F_x$ (Ln = Pr, Nd) oxypnictides reported so far which suggests that electronic disorder is considerable.[28] In this case conduction can only take place by an exchange transition to the final state so that the electron reaches its final state by an indirect, rather than a single, transition.[28] The electron percolates through the network in a set of varied jumps, rather than a single jump, and the additional energy is supplied to the electron by a multiphonon process. The double slope behavior observed for $PrMnAsO_{0.95}F_{0.05}$ has been reported in the insulating phase of high temperature superconducting cuprates[28] and also in $SrFeO_{3-\delta}$[29] and is due to multiphonon assisted hopping in different temperature regimes. Below 12 K a further electronic transition is evidenced for $PrMnAsO_{0.95}F_{0.05}$ so that variable range hopping of the electrons is no longer observed. The variation of resistivity with temperature is displayed in inset a, Figure 7, and the resistivity appears to reach a maximum at 4 K. The origin of this transition is currently unknown.

Figure 8 shows the variation of the magnetoresistance with temperature for both $PrMnAsO_{0.95}F_{0.05}$ and $NdMnAsO_{0.95}F_{0.05}$

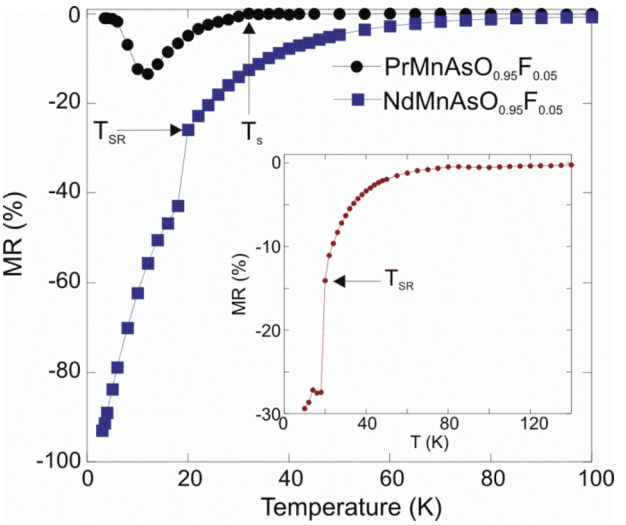

Figure 8. Temperature variation of the MR_{7T} for $PrMnAsO_{0.95}F_{0.05}$ and $NdMnAsO_{0.95}F_{0.05}$ demonstrating the absence of CMR in $PrMnAsO_{0.95}F_{0.05}$. The structural transition (T_s) observed at ~35 K for $PrMnAsO_{0.95}F_{0.05}$ and the spin reorientation transition (T_{SR}) observed at 20 K for $NdMnAsO_{0.95}F_{0.05}$ are indicated. The inset shows the temperature variation of MR_{7T} for $NdMnAsO_{0.98}F_{0.02}$.

recorded in a 7 T magnetic field. The MR of $PrMnAsO_{0.95}F_{0.05}$ is very different from that reported for $NdMnAsO_{1-x}F_x$ ($x \geq 0.05$) and there is no evidence of CMR down to 4 K. Instead, upon cooling below the structural transition at ~35 K a sizable negative MR is observed ($MR_{7T}(12K) = -13.4\%$). Below 12 K the magnitude of the −MR rapidly decreases so that by 4 K the $MR_{7T} = -0.9\%$. Below 12 K a further electronic transition is evidenced (as described earlier) so that VRH of the charge carriers is no longer observed and demonstrates that the MR is sensitive to the conduction mechanism. There is no evidence of MR above 35 K.

DISCUSSION

The magnetic properties of $NdMnAsO_{0.95}F_{0.05}$ and $PrMnAsO_{0.95}F_{0.05}$ exhibit clear differences. In both materials there is significant magnetic coupling between the lanthanide and Mn ions. In $PrMnAsO_{0.95}F_{0.05}$ the Mn spin reorientation transition and subsequent induced antiferromagnetic order of Pr^{3+} occurs below ~220 K and over a much wider temperature range (~80 K compared to 3 K in $NdMnAsO_{0.95}F_{0.05}$). The Nd antiferromagnetic transition and subsequent spin reorientation of Mn moments in $NdMnAsO_{0.95}F_{0.05}$ also occurs at a much lower temperature (23 K).[11] Density functional calculations have shown that the spin reorientation transitions observed in LnMnAsO (Ln = lanthanide) are controlled by the strength of the Dzyaloshinskii−Moriya (DM) and biquadratic (BQ) exchanges between Ln^{3+} and Mn.[30] Below the SR transition the Mn and Pr^{3+} spins are collinear so that the BQ interaction dominates over the DM interaction. The higher spin reorientation transition temperature observed in $PrMnAsO_{0.95}F_{0.05}$ compared to $NdMnAsO_{0.95}F_{0.05}$ therefore demonstrates a much stronger BQ interaction between Mn and Ln^{3+} in $PrMnAsO_{0.95}F_{0.05}$.[30]

Figure 8 shows that the MR properties of $PrMnAsO_{0.95}F_{0.05}$ are very different from those of $NdMnAsO_{0.95}F_{0.05}$ in which colossal magnetoresistance is observed at low temperature ($MR_{9T}(3K)) = -95\%$). Both materials are semiconducting with Arrhenius behavior at high temperature and variable range hoping of the charge carriers below ~80 K. However, surprisingly, the CMR observed for $NdMnAsO_{1-x}F_x$ is absent in $PrMnAsO_{0.95}F_{0.05}$. −MR is observed below ~75 K in $NdMnAsO_{0.95}F_{0.05}$, but at T_{SR} the magnitude of −MR increases sharply (Figure 8). At T_{SR}, in $NdMnAsO_{1-x}F_x$, the spin reorientation of the Mn spins (from aligning along c to aligning parallel to a) precipitates an electronic transition to Efros Shklovskii (ES) VRH. This signifies that the reorientation of Mn spins into the basal plane at 20 K results in enhanced Coulomb correlations between localized electrons,[11] which results in much higher resistivity below T_{SR}. A variable field neutron diffraction study has shown that upon applying a magnetic field there is a second order phase transition from antiferromagnetic to paramagnetic order of both the Nd and Mn spins.[11] The CMR then arises as a result of a second order phase transition from an insulating antiferromagnet to a semiconducting paramagnet upon applying a magnetic field, so that the electron correlations are diminished in field.[11] The MR at a given field, H, is related to the magnitude of the antiferromagnetically ordered Mn moment, so that $-MR = (\Delta M/C)^{1/2}$, where $\Delta M = M(0) - M(H)$, where $M(H)$ is the Mn^{2+} moment in field, $M(0)$ is the Mn^{2+} moment when $\mu_0 H = 0$ T, and C is a constant (0.4 μ_B at 4 K) which equates to the moment reduction that would theoretically result in a −MR of 100%.

The temperature variation of the MR of $PrMnAsO_{0.95}F_{0.05}$ is very different (Figure 8), and a sizable −MR is only observed below T_s. Below T_s multipolar order of the Pr 4f ground state is observed so that the sizable −MR observed most likely arises due to a reduction in magnetic and/or multipolar scattering upon application of a magnetic field. The absence of CMR in $PrMnAsO_{0.95}F_{0.05}$ is perhaps surprising and most likely suggests that the phase transition from antiferromagnetic to paramagnetic order of both the Ln and Mn spins observed from variable field neutron diffraction studies of $NdMnAsO_{0.95}F_{0.05}$ (which results in the CMR) is not evident in $PrMnAsO_{0.95}F_{0.05}$.

DOI: 10.1021/ic502445t
Inorg. Chem. 2015, 54, 2536−2542

It has previously been proposed that the antiferromagnetic to paramagnetic phase transition in $NdMnAsO_{1-x}F_x$ arises as a result of a linear coupling between a hidden order parameter and the Mn and/or Nd antiferromagnetic moments.[11] Such behavior has also been reported for the heavy Fermion material URu_2Si_2.[31] The absence of CMR in $PrMnAsO_{0.95}F_{0.05}$ would suggest that the hidden order parameter is no longer present and most likely originates from the Nd^{3+} cation. The hidden order parameter could, for example, originate from multipolar ordering of the Nd^{3+} 4f ground state. Further studies are warranted to gain a better understanding of the complex physics reported for $NdMnAsO_{0.95}F_{0.05}$. For $PrMnAsO_{0.95}F_{0.05}$, there is also no evidence of an Efros Shklovskii VRH transition (T_{ES}) down to 4 K. Hence electron correlations are weaker in $PrMnAsO_{0.95}F_{0.05}$ so that the contribution to the CMR observed in $NdMnAsO_{1-x}F_x$ below the simultaneous spin reorientation and ES transition is absent. The weaker electron correlations in $PrMnAsO_{0.95}F_{0.05}$ could be a result of the structural change from tetragonal to orthorhombic symmetry below 35 K which results in a longer Mn−As bond length along b (as the Mn moments align parallel to b below T_s). In comparison at 10 K the Mn−As bond length is 2.5424(5) Å in $NdMnAsO_{0.95}F_{0.05}$, compared to 2.556(1) Å in $PrMnAsO_{0.95}F_{0.05}$.

We note that it is unlikely that the difference in the MR behavior of $PrMnAsO_{0.95}F_{0.05}$ and $NdMnAsO_{0.95}F_{0.05}$ is a result of small differences in O:F stoichiometry. The temperature variation of the MR of $NdMnAsO_{0.98}F_{0.02}$ is very similar to that of $NdMnAsO_{0.95}F_{0.05}$, where a large drop in MR is observed at T_{SR} (Figure 8, inset). However, the overall MR is much smaller ($MR_{7T}(10K) \sim -29\%$).

CONCLUSION

Similar to $NdMnAsO_{0.95}F_{0.05}$, $PrMnAsO_{0.95}F_{0.05}$ is a semiconductor with magnetic coupling between the rare earth and Mn magnetic spins. Antiferromagnetic order of the Mn spins with moments aligned parallel to c is observed below 340 K for $PrMnAsO_{0.95}F_{0.05}$. Below 220 K the Mn spins begin to reorient into the basal plane, which subsequently induces antiferromagnetic order of the Pr spins at 180 K. However, unlike $NdMnAsO_{0.95}F_{0.05}$, a tetragonal to orthorhombic structural transition is detected below 35 K, which is driven by multipolar ordering of the Pr 4f ground state and is accompanied by a sizable negative magnetoresistance below T_s. The absence of CMR in $PrMnAsO_{0.95}F_{0.05}$ may be attributed to several factors, including the absence of Efros Shklovskii VRH as a result of weakened electron correlations due to longer Mn−As bond lengths below T_s. These results demonstrate that changing the lanthanide in 1111 $LnMnAsO_{0.95}F_{0.05}$ strongly impacts the electronic and magnetic properties so that multiple mechanisms of MR are possible in manganese oxypnictides.

AUTHOR INFORMATION

Corresponding Author

*E-mail: a.c.mclaughlin@abdn.ac.uk.

Notes

The authors declare no competing financial interest.

ACKNOWLEDGMENTS

This research is supported by the EPSRC (Research Grant EP/L002493/1). We also acknowledge STFC-GB for provision of beamtime at ILL and ESRF.

REFERENCES

(1) Kamihara, Y.; Watanabe, T.; Hirano, M.; Hosono, H. *J. Am. Chem. Soc.* **2008**, *130*, 3296−3297.
(2) Johnston, D. C. *Adv. Phys.* **2010**, *59*, 803−1061.
(3) Chen, G. F.; Li, Z.; Wu, D.; Dong, J.; Li, G.; Hu, W. Z.; Zheng, P.; Luo, J. L.; Wang, N. L. *Chin. Phys. Lett.* **2008**, *25*, 2235−2238.
(4) Ren, Z. A.; Yang, J.; Lu, J. W.; Yi, W.; Che, G. C.; Dong, X. L.; Sun, L. L.; Zhao, Z. X. *Mater. Res. Innovations* **2008**, *12*, 105−106.
(5) Pottgen, R.; Johrendt, D. *Z. Naturforsch.* **2008**, *63b*, 1135−1148.
(6) Ren, Z. A.; Che, G.-C.; Dong, X.-L.; Yang, J.; Lu, W.; Yi, W.; Shen, X.-L.; Li, Z.-C.; Sun, L.-L.; Zhou, F.; Zhao, Z.-X. *Europhys. Lett.* **2008**, *83*, No. 17002.
(7) Wang, C.; Li, L.; Chi, S.; Zhu, Z.; Ren, Z.; Li, Y.; Wang, Y.; Lin, X.; Luo, Y.; Jiang, S.; Xu, X.; Cao, G.; Xu, Z. *Europhys. Lett.* **2008**, *83*, No. 67006.
(8) Emery, N.; Wildman, E. J.; Skakle, J. M. S.; Mclaughlin, A. C. *Phys. Rev. B* **2011**, *83*, No. 144429.
(9) Yanagi, H.; Kawamura, R.; Kamiya, T.; Kamihara, Y.; Hirano, M.; Nakamura, T.; Osawa, H.; Hosono, H. *Phys. Rev. B* **2008**, *77*, No. 224431.
(10) Watanabe, T.; Yanagi, H.; Kamihara, Y.; Kamiya, T.; Hirano, M.; Hosono, H. *J. Solid State Chem.* **2008**, *181*, 2117−2120.
(11) Wildman, E. J.; Skakle, J. M. S.; Emery, N.; Mclaughlin, A. C. *J. Am. Chem. Soc.* **2012**, *134*, 8766−8769.
(12) Rao, C. N. R., Raveau, B., Eds. *Colossal Magnetoresistance, Charge Ordering and Related Properties of Manganese Oxides*; World Scientific: Singapore, 1998.
(13) Ramirez, A. P. *J. Phys.: Condens. Matter* **1997**, *9*, No. 8171.
(14) Jin, S.; Tiefel, T. H.; McCormack, M.; Fastnacht, R. A.; Ramesh, R.; Chen, L. H. *Science* **1994**, *264*, 413−415.
(15) Yin, R.; Yo, C. H. *J. Mater. Sci.* **2007**, *42*, 660−668.
(16) Subramanian, M. A.; Toby, B. H.; Ramirez, A. P.; Marshall, W. J.; Sleight, A. W.; Kwei, G. H. *Science* **1996**, *273*, 81−84.
(17) Marcinkova, A.; Hansen, T. C.; Curfs, C.; Margadonna, S.; Bos, J.-W. G. *Phys. Rev. B* **2010**, *82*, No. 174438.
(18) Emery, N.; Wildman, E. J.; Skakle, J. M. S.; Giriat, G.; Smith, R. I.; Mclaughlin, A. C. *Chem. Commun. (Cambridge, U. K.)* **2010**, *46*, 6777−6779.
(19) Hanna, T.; Matsuishi, S.; Kodama, K.; Otomo, T.; Shamoto, S.-I.; Hosono, H. *Phys. Rev. B* **2013**, *87*, No. 020401.
(20) Shiomi, Y.; Ishiwata, S.; Taguchi, Y.; Tokura, Y. *Phys. Rev. B* **2011**, *84*, No. 054519.
(21) Nientiedt, A. T.; Jeitschko, W.; Pollmeier, P. G.; Brylak, M. *Z. Naturforsch.* **1997**, *52b*, 560−564.
(22) Rietveld, H. M. *Acta Crystallogr.* **1967**, *22*, 151−152.
(23) Larson, A. C.; Von Dreele, R. B. *General Structure Analysis System (GSAS)*, Technical Report No. LAUR 86-748; Los Alamos National Laboratory: Los Alamos, NM, USA, 2004; https://subversion.xor.aps.anl.gov/EXPGUI/gsas/all/GSAS%20Manual.pdf.
(24) Kimber, S. A. J.; Hill, A. H.; Zhang, Y.; Jeschke, H. O.; Valentí, R.; Ritter, C.; Schellenberg, I.; Hermes, W.; Pöttgen, R.; Argyriou, D. N. *Phys. Rev. B* **2010**, *82*, No. 100412(R).
(25) Tsukamoto, Y.; Okamoto, Y.; Matsuhira, K.; Whangbo, M.-H.; Hiroi, Z. *J. Phys. Soc. Jpn.* **2011**, *80*, No. 094708.
(26) Mott, N. F. *Metal-Insulator Transitions*; Taylor and Francis: London, 1974.
(27) Mott, N. F.; Davis, E. A. *Electronic Processes in Non-Crystalline Materials*; Clarendon: Oxford, U.K., 1979.
(28) Prabhu, P. S.; Ramachandra Rao, M. S.; Varadaraju, U. V.; Subba Rao, G. V. *Phys. Rev. B* **1994**, *50*, 6929−6938.
(29) Srinath, S.; Kumar, M. M.; Post, M. L.; Srikanth, H. *Phys. Rev. B* **2005**, *72*, No. 054425.
(30) Lee, C.; Kan, E.; Xiang, H.; Kremer, R. K.; Lee, S.-H.; Hiroi, Z.; Whangbo, M.-H. *Inorg. Chem.* **2012**, *51*, 6890−6897.
(31) Bourdarot, F.; Fåk, B.; Habicht, K.; Prokes, K. *Phys. Rev. Lett.* **2003**, *90*, No. 067203.

DOI: 10.1021/ic502445t
Inorg. Chem. 2015, 54, 2536−2542